PREPARATION, THERMAL, SPECTRAL AND MICROSCOPIC STUDIES OF CALCIUM SILICATE HYDRATE–POLY(ACRYLIC ACID) NANOCOMPOSITE MATERIALS

S. C. Mojumdar[*] *and L. Raki*

Institute for Research in Construction, National Research Council of Canada, M-20, 1200 Montreal Road, Ottawa, Ontario K1A 0R6 Canada

A series of calcium silicate hydrate (C–S–H)-polymer nanocomposite (C–S–HPN) materials were prepared by incorporating poly(acrylic acid) (PAA) into the inorganic layers of C–S–H during precipitation of quasicrystalline C–S–H from aqueous solution. The as-synthesized C–S–HPN materials were characterized by X-ray fluorescence (XRF), X-ray diffraction (XRD), scanning electron microscopy-energy dispersive spectroscopy (SEM-EDS), Fourier-transform infrared (FTIR) spectroscopy, thermogravimetric analysis (TG) and differential scanning calorimetry (DSC). The XRD analysis of C–S–HPN materials suggest the intermediate organizations presenting intercalation of PAA within C–S–H and exfoliation of C–S–H. The SEM micrographs of C–S–H, PAA and C–S–HPN materials with different PAA contents exhibit the significant differences in their morphologies. The effect of the material's composition on the thermal stability of a series of C–S–HPN materials along with PAA and C–S–H were studied by TG, DTA and DSC. Three significant decomposition temperature ranges were observed on the TG curves of all C–S–HPN materials.

Keywords: C–S–H, C–S–HPN nanocomposites, DSC, DTA, FTIR spectroscopy, PAA, SEM, TG

Introduction

Calcium silicates hydrate (C–S–H) is the main hydrated phase in cement paste. It has a nanocrystalline layered structure and possesses hydraulic properties [1]. Poly(acrylic acid) (PAA), a carboxylic acids polymer, is known to react with multivalent metal cations and forms crosslinks with metals, which are insoluble in water and most of the organic solvents. For such polymers, Coulomb force, the strongest interaction, works between molecules and metal ions, hence it is considered to have an excellent potential as materials with high modulus, high strength and high heat resistance in the solid-state [2]. Therefore, PAA was used to synthesize C–S–HPN materials with improved properties. Nanocomposite materials consisting of inorganic nanolayers of C–S–H and organic polymers have evoked intense research interest lately because their unique characteristics create many potentially commercial applications. The synthesis of C–S–H-based nanocomposites using a number of organic polymers was recently reported [3–7].

Composites are already widely used in such diverse as transportation, construction, electronics and consumer products. They offer unusual combinations of stiffness, strength and mass that are difficult to attain separately from individual components [8]. On the other hand nanocomposites are a relatively new class of materials and are defined as particle-filled polymers with ultrafine phase dimensions, typically of the order of a few nanometers [9]. Because of their nanometer size features nanocomposites possess unique properties typically not shared by their more conventional microcomposite counterparts and, therefore offer new technology and business opportunities [7–16].

Organic–inorganic hybrid materials, composed of layered inorganic matrix with organic polyconjugated macromolecules in the interlayer space, have been the subjects of thorough attention of researchers for the past 5–15 years [17–46]. One of the very important materials of this type is so-called macro-defect-free (MDF) material at microscopic and nano-metric levels [47]. Polymers are very important additives in the manufacture and processing of various materials, where the modification of interfaces and particles surface functionalisations are largely influenced by the model of functional polymer. The theory of functional polymer, modification of a surface by grafting/reaction of polymer chains to/with the surface of and inorganic materials are discussed in [48, 49].

In this study the focus is on the design and synthesis of C–S–H-polymer nanocomposite materials with layered silicate as the inorganic phase. The approach exploits the ability of C–S–H (layered silicates) to intercalate between their layers a wide variety of polymers [5–7]. Due to the layer orientation, polymer-sili-

_____
* Author for correspondence: subhash.mojumdar@nrc-cnrc.gc.ca

cate nanocomposites also exhibit stiffness, strength and dimensional stability in two dimensions (rather than one). In addition, because of the length scale involved that minimizes scattering, nanocomposites are usually transparent. Furthermore, C–S–HPN materials exhibit a significant increase in thermal stability as well as self-extinguishing characteristics [1–16]. Organic–inorganic nanocomposite materials are reported to promote thermal [50, 51], mechanical [52], molecular barriers [53], flame retardant behavior [54–61] and corrosion protection properties [62–64]. Therefore, the systematic investigation of the reaction possibility of PAA with synthetic C–S–H at low Ca/Si ratio (0.7) as well as to characterize the nanocomposite materials by nanotechnological methods are the main interests of this contribution.

Experimental

Materials

Poly(acrylic acid)-partial Na-salt ([–$CH_2CH(CO_2R)$–]$_n$, R=H or Na), (M_W=5000 (Aldrich Chemical Company, Inc., Milwaukee, WI, USA), $Na_2SiO_3 \cdot 9H_2O$ (National Silicates, Toronto Canada), $Ca(NO_3)_2 \cdot 4H_2O$ and NaOH (Fisher Scientific, Fair Lawn, New Jersey, USA) were used to synthesize C–S–H and C–S–HPN materials.

Synthesis of C–S–HPN materials

C–S–H and C–S–HPN materials with PAA contents of (0.0 and 0.15 or 0.3 g/g Ca salt) were synthesized by gradually adding calcium nitrate solution (1 mol L^{-1}) with continual stirring under nitrogen to sodium silicate solution, which was predissolved with PAA (only for the synthesis of C–S–HPN materials) in CO_2-free de-ionized water. The initial Ca/Si molar ratio was 0.7 for C–S–H and all C–S–HPN materials. The pH value was kept between 13.2–13.4 by adding NaOH solution (5.0 M) during the precipitation of C–S–H. After aging the suspension at 60°C for seven days with continuous stirring, the precipitate was separated by vacuum filtration and washed with CO_2-free de-ionized water to remove sodium and nitrate ions and any residual PAA. The precipitates were then washed with acetone and dried at 60°C in a vacuum oven for 7 days. The synthetic C–S–H and C–S–HPN materials are summarized in Table 1.

Table 1 Synthetic C–S–H and C–S–HPN materials (Ca/Si=0.70)

Materials	PAA content (g/g Ca salt)
C–S–H (0.7)	0.0
C–S–H–PAA (0.7–0.15)	0.15
C–S–H–PAA (0.7–0.3)	0.30

Analytical methods

The powder X-ray diffraction (XRD) patterns were performed on a Scintag XDS 2000 X-ray diffractometer using CuK_α radiation at 45 kV and 35 mA between 4 and 65° (2θ) with a graphite secondary monochromator.

XRF analysis was performed on fusion beads made of 10 g of flux with a 66% lithium tetraborate 33% lithium metaborate fusion matrix and 1 g of sample. Beads were mounted into a Brukar AXS S4 Pioneer automated XRF machine and analyzed for all elements as oxides. Samples were run under vacuum and using the default peak fitting program. Results were presented as percentages by mass of the oxide version of each element detected and normalized to 100%. Loss on ignition or material loss during the fusion process was ignored during the analysis of the results due to the highly variable polymer content of the materials being tested.

Thermal analyses (TG, DTA and DSC) on powder samples (~20 mg) were carried out using a simultaneous SDT Q600 T.A.I. instrument at 10°C min^{-1} from room temperature (rT) to 1000°C under nitrogen atmosphere using a flowing rate 100 mL min^{-1}.

FTIR spectra were collected on a Bomem MB 100 spectrometer in direct transmission mode between 4000 and 400 cm^{-1} as the average of 50 scans and a 4 cm^{-1} resolution. Samples were grounded to a fine powder with KBr and pressed into a disk with a 10-ton ring press. Air was used as a background for all measurements.

SEM images were acquired on a Hitachi S-4800 Field Emission Scanning Electron Microscope. Surface structure images were taken using a beam current of 2.0 keV at 10 μA. Images were acquired using an integrated frame capture with 32 frames to reduce random noise. Images were acquired at a working distance of 8 mm and each area of interest was captured a series of field magnifications from 5000 to 80000× magnification.

Energy dispersive spectrometry (EDS) was used to determine the elemental content of areas of interest. The EDS spectra were captured using a beam current of 20 keV at 10 μA. Spectral images and data were performed at a working distance of 15 mm. Semi-quantitative results were based on ZAP software database reference values and are an indication of relative elemental content rather than absolute values as no reference standards were used.

Results and discussion

Chemical analysis

The chemical composition of C–S–H and C–S–HPN materials were determined by XRF (Table 2) and EDS (Table 3) analysis. The fusion process has been used for XRF analysis. The fusion process is an excellent

Table 2 XRF results of C–S–H and C–S–HPN materials (Ca/Si=0.70)

	C–S–H	C–S–H–PAA (0.7–0.15)	C–S–H–PAA (0.7–0.3)
SiO_2	59.17	59.66	63.66
CaO	40.83	40.34	36.59
Ca/Si molar ratio	0.74	0.72	0.70

Table 3 EDS results of a C–S–HPN material (C–S–H–PAA (0.7–0.3)) on various zones

Zone	C/%	O/%	Na/%	Si/%	Ca/%	Total/%
1	4.89	50.98	7.78	18.51	17.84	100.00
2	5.78	50.55	7.53	18.80	17.35	100.00
3	5.88	50.29	7.41	18.77	17.65	100.00
4	4.89	50.55	7.48	19.18	17.92	100.00
5	5.20	50.35	7.43	18.96	18.06	100.00

way to get quantifiable elemental analysis and the fusion beads are resistant to change so they can be stored and reanalyzed at any time. However, the process requires heating the material to over 1000°C so any volatile components such as hydrate water, carbon, sulfur or nitrates are often burned off in the fusion process. It is a very good method to determine the Ca/Si ratio. The Ca/Si ratios of C–S–H and C–S–HPN materials confirmed the theoretical expectation (0.7). But if the samples contain polymer (carbon based), nitrates and sulfates it is not a good method for quantification of all components especially carbon, nitrates and sulfates. Therefore, EDS analysis has also been carried out on various zones of C–S–H and C–S–HPN materials to determine mainly the carbon content in C–S–HPN materials. The results of EDS analysis of a C–S–HPN material on various zones are given in Table 3 as an example. The EDS result for other samples are in the same accuracy range.
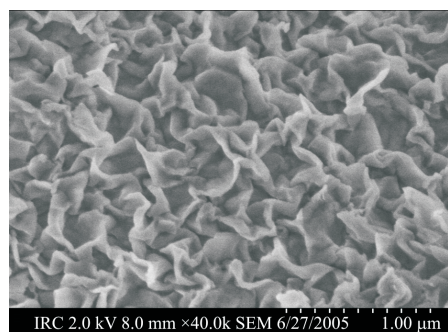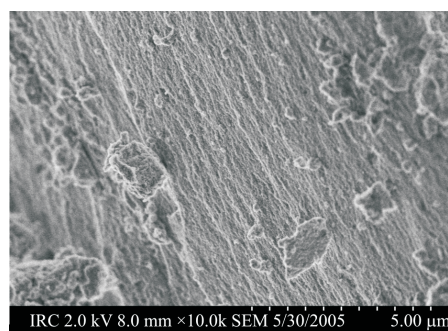
X-ray diffraction analysis

The XRD studies were performed for both C–S–H and C–S–HPN materials. The most important powder XRD peaks have been exhibited at 2θ=5–9° (XRD patterns are not shown here) (interlayer spacing *d*=1.22 nm for C–S–H and 1.30–1.40 nm for C–S–HPN materials). The XRD peaks of C–S–HPN materials not only have shifted to the lower angles but also have broadened. This behavior suggests the intermediate organizations presenting both intercalation and exfoliation. The overall C–S–H layers expansion was smaller compared to PAA molecules diameter. The formation of these nanocomposites depends on the structure of the host material itself, the charge density on the surface (here the Ca/Si ratio), the method of preparation (in-situ or exchange), and

the type of organic polymers. The small expansion upon intercalation could only be explained by a single linear extension conformation of PAA molecules [2–4]. The intermediate organizations, which present both intercalation and exfoliation have also been confirmed by SEM.

SEM analysis

The SEM images of C–S–H and C–S–HPN materials are shown on Figs 1 and 2. Figure 1 represents a SEM image of pure C–S–H. The particles display a sinuous surface, typical for C–S–H [65]. A SEM micrograph of a C–S–HPN material, which highlights the intercalated structure, has been presented in Fig. 2 (PAA=0.15 g/g Ca salt).

Fig. 1 SEM micrographs of synthetic C–S–H

Fig. 2 SEM micrographs of intercalated C–S–HPN material (C–S–H–PAA (0.7–0.15))

FTIR spectral analysis

The most significant FTIR spectral bands of C–S–H, PAA and selected C–S–HPN materials have been given in Table 4. All FTIR spectra of C–S–H and C–S–HPN materials contain characteristic bands at the range 973–978 cm^{-1}. These are the most intensive bands in all spectra and can be assigned to Si–O stretching vibration of the Q^2 tetrahedra. The weak band at 811 cm^{-1} in C–S–H spectra is assigned to Si–O stretching vibrations of the Q^1 tetrahedra (characteristic for monomeric structure). This peak is missing in all C–S–HPN materials suggesting the polymeric struc-

Table 4 The most important FTIR spectral data (4000–400 cm^{-1}) of C–S–H, PAA and C–S–HPN materials

Assignments	C–S–H/cm^{-1}	C–S–H–PAA (0.7–0.15)/cm^{-1}	C–S–H–PAA (0.7–0.3)/cm^{-1}	PAA/cm^{-1}
Si–O	973, 811	975	978	–
Si–O–Si	670	669	671	–
Si–OH	3742	3740	3741	–
H–O–H	1645	1595	1593	–
O–H	3390	3443	3445	3735
C–H	–	2935	2934	2925
C=C	–	2856	2857	2316
C=O	–	1636	1639	1744
C–O	–	1385	1385	1228
CO_3^{2-}	1431	1417	1426	
other bands	448	453	452	

ture. The Si–O–Si bands at 669–671 cm^{-1} have increased in intensity with the increasing polymer contents. The bands at 3740–3742 cm^{-1} are due to Si–OH stretching in the isolated Si–OH species. The most striking feature of the FTIR spectra is the decreasing intensity of the bands with increasing polymer contents, suggests a progressively decreasing concentration of Si–OH group. These are the key information of the structure of C–S–H and C–S–HPN materials. The stretching bands at 3390–3445 cm^{-1} can be attributed to water molecules in C–S–H and C–S–HPN materials. The bands in the range of 1593–1645 cm^{-1} are due to H–O–H bending vibrations of H_2O molecules. Other bands at 448–452 cm^{-1} are due to the internal deformation of SiO_4 tetrahedra. The bands in the range of 1417–1431 cm^{-1} correspond to the asymmetric stretching (v_3) of CO_3^{2-} (it is not possible to prevent incorporation of CO_2 during sample preparation) [66].

The characteristic vibration bands of PAA and C–S–HPN materials are observed at 3240–3337 cm^{-1} (–OH), 2857–2891 cm^{-1} (–CH_2), 1410–1445 cm^{-1} (O=C–OR), 1035–1093 cm^{-1} (C–O–C) and 831–844 cm^{-1} (–CH) [67]. Since the stretching vibrations of (O=C–OR) and CO_3^{2-} appear at very close region, these two bands overlapped and become one peak in the spectra of C–S–HPN materials. The presence of PAA bands in C–S–HPN materials is the indication of the presence of PAA molecules within C–S–H, as it is also supported by XRD and SEM results.

TG, DTA and DSC studies of C–S–H, PAA and C–S–HPN materials

The most important thermoanalytical (TG, DTA and DSC) data of C–S–H, representative C–S–HPN materials and bulk PAA are presented in Table 5. Figure 3 shows the TG curves of C–S–H, PAA and representative C–S–HPN materials. There are significant differ-

ences in the thermal decomposition properties of C–S–H, PAA and C–S–HPN materials. C–S–HPN materials exhibit higher thermal stability compared to starting materials (C–S–H and PAA).

In general, three (for PAA) and two (for C–S–H and C–S–HPN materials) significant temperature regions on TG curves have been observed:

- Region I (rT–350°C): this is the region of bound water removal [63–68] due to the loss of molecular water with DTA peaks at 71–235°C (Table 5, Fig. 3). In the case of C–S–HPN materials, the decomposition temperature (T_d) in this region is variable depending on the synthesis and material compositions (Table 5, Fig. 3). For pure PAA, this temperature region has divided into two regions: rT–150 and 150–250°C with two DTA peaks at 116 and 235°C, respectively. The first and second temperature regions and DTA peaks are due to the absorbed and bound water removal, respectively [69, 70].
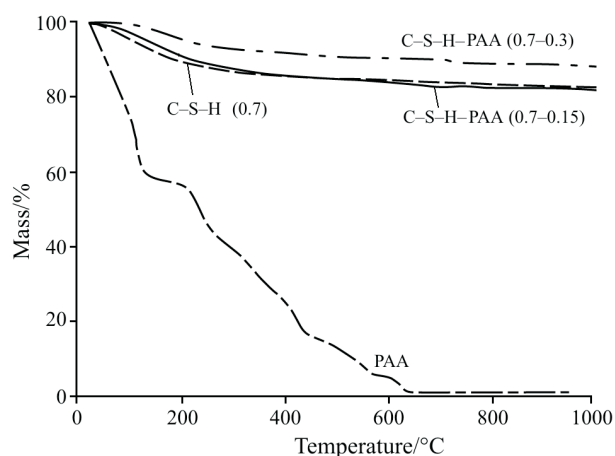

Fig. 3 TG curves of C–S–H, PAA and C–S–HPN materials with different polymer contents

Table 5 Summary of thermal analysis data for C–S–H, PAA and C–S–HPN materials

Compound	$T_d/°C$	DTA peak/°C	$T_g/°C$
C–S–H	250, over 550	71, 693	87
C–S–H–PAA (0.7–0.15)	250, 550, over 550	136, 761	142
C–S–H–PAA (0.7–0.3)	350, 550, over 550	143, 773	154
PAA	150, 250, 437, 550, over 550	116, 235, 402, 496, 585	106

T_d=decomposition temperature, T_g=glass transition temperature

- Region II (250–550°C): this temperature region is attributed mainly to the polymeric material decomposition [68–74]. For PAA, two decomposition steps are observed (Table 5, Fig. 3). DTA curve of PAA exhibits two DTA peaks at 402 and 496°C (Table 5). The first and second temperature regions and DTA peaks are due to the decomposition of carboxyl groups [70]. However, C–S–HPN materials exhibit no significant decomposition step and no DTA peak in this region. This fact strongly suggests that carboxyl groups of PAA have reacted with C–S–H, and decomposition of carboxyl groups has not occurred in this temperature region.
- Region III (over 550°C): this temperature region is characteristic for rupture of the polymer chain [70] and structural water decomposition [71–78] with DTA peak temperature in 585–773°C range.

DSC traces of C–S–H, PAA and C–S–HPN materials are presented in Fig. 4. PAA exhibits an endotherm at 106°C corresponding to the glass transition temperature (T_g) of PAA. T_g depends on the molecular structure of the polymer (chain stiffness, number and bulkiness of the side groups, and the inter- and intra-molecular interactions) and on the cross-link density of the polymer [79]. All the C–S–HPN materials are found to have higher T_g compared to that of C–S–H and bulk PAA, as shown in Table 5 and Fig. 4. This behaviour is tentatively attributed to the confinement of the intercalated polymer chains within the C–S–H galleries that prevents the segmental motions of the polymer chains. The DSC peaks of C–S–HPN materials shift to higher temperatures suggesting the intercalation of PAA into C–S–H. The largest shift of the endotherm (toward the higher temperature) occurs on the DSC curve of C–S–HPN material containing PAA 0.3 (g/g Ca salt). This fact suggests the greatest intercalation of the PAA molecules.

Conclusions

We have presented several examples of polymer nanocomposites with calcium silicate hydrate (layered silicate) as the inorganic phase. The materials design and synthesis rely on the ability of layered silicates to intercalate a wide range of polymers in the galleries between their layers. Special emphasis has been given on a new, versatile and environmentally benign synthesis approach by solution intercalation. New calcium silicate hydrate/poly(acrylic acid) nanocomposite (C–S–HPN) materials, synthesized by solution technique have been characterized by XRD, XRF SEM-EDS, TG, DTA, DSC and FTIR spectra. The XRD and SEM results suggest the intercalation of PAA within C–S–H. Significant differences in the morphologies of C–S–H and C–S–HPN materials with different PAA contents have been observed in SEM micrographs. The influence of the material's compositions on the thermal decomposition of C–S–HPN materials along with pure PAA and synthetic C–S–H has been studied by TG, DTA and DSC. The C–S–HPN materials exhibit significant increase in thermal stability compared to that of C–S–H and PAA.

This investigation introduces new routes for developing cement-based nanocomposite materials with various polymers for future potential applications in the construction field. A study to elucidate the effect of PAA molecules intercalation on Ca/Si ratio of C–S–HPN materials by means of thermal conductivity, TMA, XPS, NMR spectra, TEM and AFM microscopy will be presented in a future contribution.
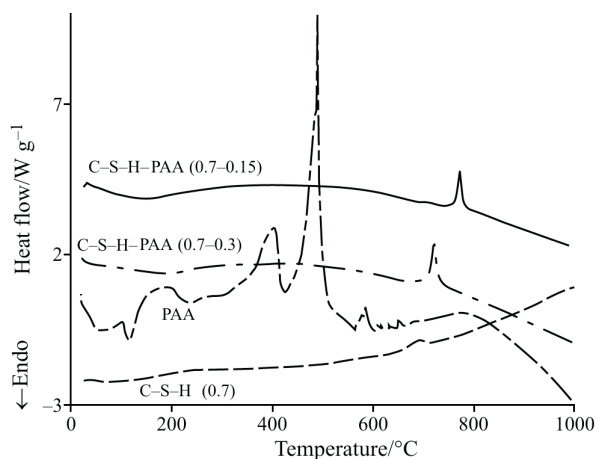

Fig. 4 DSC curves of C–S–H, PAA and C–S–HPN materials with different polymer contents

References

1 H. Matsuyama and J. F. Young, J. Mater. Res., 14 (1999) 3379.

2 Y. Gotoh, Y. Ohkoshi and M. Nagura, Transaction, 55 (1999) 522.

3 H. Matsuyama and J. F. Young, J. Mater. Res., 14 (1999) 16.

4 H. Matsuyama and J. F. Young, Chem. Mater., 11 (1999) 3389.

5 S. C. Mojumdar and L. Raki, J. Therm. Anal. Cal., 82 (2005) 89.

6 S. C. Mojumdar and L. Raki, Preparation and Properties of Calcium Silicate Hydrate Polymer Nanocomposite, 107th American Ceramics Society Annual Meeting, Exposition and Technology Fair, Baltimore, MD, USA April 10–13, 2005.

7 S. C. Mojumdar and L. Raki, J. Therm. Anal. Cal., 82 (2005) 89.

8 E. P. Giannelis, Adv. Mater., 8 (1996) 29.

9 M. Alexandre and P. Dubois, Mater. Sci. Eng., 28 (2000) 1.

10 J. E. Mark, Polym. Eng. Sci., 36 (1996) 2905.

11 E. Reynaud, C. Gauthier and J. Perez, Rev. Metall./Cah. Inf. Tech., 96 (1999) 169.

12 T. Von Werne and T. E. Patten, J. Am. Chem. Soc., 121 (1999) 7409.

13 N. Heron and D. L. Thorn, Adv. Mater., 10 (1998) 1173.

14 P. Cavert, Potential application of nanotubes, in: T. W. Ebbesen (Ed.), Carbon Nanotubes, CRC Press, Boca Raton, FL 1997, pp. 277–292.

15 V. Favier, G. R. Canova, S. C. Shrivastava and J. Y. Cavaille, Polym. Eng. Sci., 37 (1997) 1732.

16 L. Chazeau, J. Y. Cavalle, G. Canova, R. Dendievel and B. Boutherin, J. Appl. Polym. Sci., 71 (1999) 1797.

17 M. Delucchi and G. Cerisola, Constr. Build. Mater., 15 (2001) 351.

18 M. G. Kanatzidis and L. M. Tonge, J. Am. Chem. Soc., 109 (1987) 3797.

19 M. Drábik, L. Gáliková, K. G. Varshney and M. A. Quraishi, J. Therm. Anal. Cal., 76 (2004) 91.

20 G. K. D. Pushpalal, J. Mater. Sci., 35 (2000) 981.

21 B. X. Li, W. Q. Liang, W. S. Zhang and Z. He, J. Chin. Cer. Soc., 28 (2000) 325.

22 S. C. Mojumdar, J. Therm. Anal. Cal., 64 (2001) 1133.

23 J. D Birchal, A. J. Howard, K. Kendal and J. H. Raistrick, 1988, June, Cementitious Composition and Cementitious Product of High Flexural Strength, European Pat. Specification, B1, No. 0055035, pp. 1–17.

24 M. Drabik, S. C. Mojumdar and L. Galikova, Cem. Concr. Res., 31 (2001) 751.

25 J.A. Lewis and P.G. Desai, 1996, MAETA Workshop on High Flexural Polymer-Cement Composite, Sakata 3–4 October, pp. 49–58.

26 S. C. Mojumdar and M. Drabik, Science of cement and concrete-Kurdowski Symposium (Akapit Scientific Publisher, Poland 2001).

27 S. C. Mojumdar, A. Ray, M. Drábik, A. Cigan, F. Hanic and P. Capek, Sol. Stat. Phenom., 90–91 (2003) 365.

28 M. Drabik, L. Galikova and S. C. Mojumdar, Key Eng. Mater., 206–213 (2002) 1867.

29 S. C. Mojumdar, Thermophysics 2001, October 23–25, 2001, Račková Dolina, High Tatras, Slovakia, pp. 93–98.

30 K. Kendal, A. J. Howard and J. D. Birchal, Philos. Trans. R. Soc., A310 (1983) 139.

31 M. Drábik, S. C. Mojumdar and R. C. T. Slade, CERAMICS – Silikaty, 46 (2002) 68.

32 B. X. Li, W. Q. Liang and Z. He, J. Wuhan Univ. Technol., 16 (2001) 25.

33 S. C. Mojumdar and L. Raki, Res. J. Chem. Environ., submitted.

34 M. Delucchii and G. Cerisola, Constr. Build. Mater., 15 (2001) 351.

35 S. C. Mojumdar, Challenges for Coord. Chemistry in the new century, 5 (2001) 453.

36 R. Alfani, P. Colombet, A. D'Amore, N. Rizzo and L. Nicolais, J. Mater. Sci., 34 (1999) 5683.

37 S. C. Mojumdar, Res. J. Chem. Environ., 9 (2005) 23.

38 C. Y. Rha, J. W. Seong, C. E. Kim, S. K. Lee and W. K. Kim, J. Mater. Sci., 34 (1999) 4653.

39 C. K. Park, J. Ceram. Soc. Jpn., 106 (1998) 268.

40 J. A. Lewis and M. A. Boyer, Adv. Cem. Bas. Mater., 2 (1995) 2.

41 M. Tan, J. Lu and K. Wu, Cem. Concr. Res., 24 (1994) 1185.

42 P. G. Desai, J. A. Lewis and D. P. Bentz, J. Mater. Sci., 29 (1994) 711.

43 I. A. A. Ibrahim, H. H. El Sersy and M. F. Abadir, J. Therm. Anal. Cal., 76 (2004) 713.

44 J. Dweck, P. F. Ferreira da Silva, R. Silva Aderne, P. M. Büchler and F. K. Cartledge, J. Therm. Anal. Cal., 71 (2003) 821.

45 S. C. Mojumdar, B. Chowdhury, K. G. Varshney and K. Mazanec, J. Therm. Anal. Cal., 78 (2004) 135.

46 T. Lan, P. D. Kaviratna and T. J. Pinnavaia, Chem. Mater., 6 (1994) 573.

47 I. Odler, Special Inorganic Cement, Capter 13.3, MDF cement, E & F. N. Spon, London, New York 2000.

48 G. Wegner, Acta Materialia (The millennium special issue), 48 (2000) 253.

49 M. Drabik and R.C.T. Slade, Interf. Sci., 12 (2004) 375.

50 M. Zanetti, P. Bracco and L. Costa, Polym. Degrad. Stab., 85 (2004) 657.

51 H.-L. Tyan, Y.-C. Liu and K.-H. Wei, Chem. Mater., 11 (1999) 1942.

52 Z. Wang and T. J. Pinnavaia, Chem. Mater., 10 (1998) 3769.

53 J. Liu, Y. Gao, F. Wang and W. Ming, J. Appl. Polym. Sci., 75 (2000) 384.

54 J. W. Gilman, Appl. Clay Sci., 15 (1999) 31.

55 J. W. Gilman, C. L. Jackson, A. B. Morgan, J. R. Hayyis, E. Manias, E. P. Giannelis, M. Wuthenow, D. Hilton and S. H. Philips, Chem. Mater., 12 (2000) 1866.

56 D. Porter, E. Metcalfe and M. J. K. Thomas, Fire Mater., 24 (2000) 45.

57 J. Wang, J. Dua, J. Zhu and C. A. Wilkie, Polym. Degrad. Stab., 77 (2002) 249.

58 M. Zanetti, G. Camino, D. Canavese, A. B. Morgan, F. J. Lamelas and C. A. Wilkie, Chem. Mater., 14 (2002) 189.

59 M. Zanetti, T. Kashiwagi, L. Falqui and G. Camino, Chem. Mater., 14 (2002) 881.

60 J. Zhu, P. Start, K. A. Mauritz and C. A. Wilkie, Polym. Degrad. Stab., 77 (2002) 253.

61 J. Zhu, F. Uhl, A. B. Morgan and C. A. Wilkie, Chem. Mater., 13 (2001) 4649.

62 J. M. Yeh, S. J. Liou, C. Y. Lai, P. C. Wu and T. Y. Tsai, Chem. Mater., 13 (2001) 1131.

63 J. M. Yeh, C. L. Chen, Y. C. Chen, C. Y. Ma, K. R. Lee, Y. Wei and S. Li, Polymer, 43 (2002) 2729.

64 J. M. Yeh, S. J. Liou, C. Y. Lin, C. Y. Cheng, Y. W. Chang and K. R. Lee, Chem. Mater., 14 (2002) 154.

65 I. Pointeau, B. Piriou, M. Fedoroff, M. G. Barthes, N. Marmier and F. Fromage, J. Coll. Inter. Sci., 236 (2001) 252.

66 P. Yu, R. J. Kirkpatrick, B. Poe, P. F. McMillan and X. Cong, J. Am. Ceram. Soc., 82 (1999) 742.

67 G. Cardenas, C. Munoz and H. Carbacho, Eur. Polym. J., 36 (2000) 1091.

68 B. Chowdhury, J. Therm. Anal. Cal., 78 (2004) 215.

69 X.-D. Fan, Y.-L. Hsieh, J. M. Krochta and M. J. Kurth, J. Appl. Polym. Sci., 82 (2001) 1921.

70 N. Sebastian, B. George and B. Mathew, Polym. Degrad. Stab., 60 (1998) 371.

71 M. Drabik, L. Galikova, F. Hanic and J. H. Sharp, Chem. Papers, 51 (1997) 363.

72 M. Drabik, L. Galikova and P. Zimermann, J. Therm. Anal. Cal., 56 (1999) 117.

73 I. Janotka and L'. Krajči, Bul. Mater. Sci., 23 (2000) 521.

74 H. F. W. Taylor, Cement Chemistry, 2nd Edn. (Thomas Telford Publ., London 1998).

75 I. Janotka, L'. Krajči, A. Ray and S. C. Mojumdar, Cem. Concr. Res., 33 (2003) 489.

76 C. A. Strydom and J. H. Potgieter, An investigation into the chemical nature of the reactivity of lime, Proc. 10th Int. Congr. Chem. Cement (Ed. H. Justnes, Sweden 1997).

77 I. Janotka and S. C. Mojumdar, Sol. Stat. Phenom., 90–91 (2003) 309.

78 I. Janotka, T. Nürnbergerová and L. Nad, Magaz. Concr. Res., 52 (2000) 399.

79 S. J. Kim, K. J. Lee, S. M. Lee, I. Y. Kim, Y. M. Lee and S. I. Kim, J. Appl. Polym. Sci., 88 (2003) 2670.